Improving HWRF Track and Intensity Forecasts via Model Physics Evaluation and Tuning

Robert G. Fovell and Yizhe Peggy Bu

Department of Atmospheric and Oceanic Sciences

University of California, Los Angeles

rfovell@ucla.edu

DTC Visitor Program final report

1. Background

We have appreciated for some time that microphysical assumptions can dramatically influence tropical cyclone (TC) intensity (e.g., Lord et al. 1984; Braun and Tao 2000; Wang 2002; Zhu and Zhang 2006). Fovell and Su (2007) were among the first to show that cloud processes could materially influence TC motion over periods as short as two days. Using a "semi-idealized" strategy (i.e., employing operational models with dramatically simplified initial conditions), Fovell et al. (2009) demonstrated that different microphysical parameterizations (MPs) tend to generate different storm structures, particularly with regard to the azimuthally-averaged winds in the TC's outer core region, located 200 km or more from the center. These outer winds can influence motion via the "beta drift" (e.g., Holland 1983; Fiorino and Elsberry 1989). Indeed, Cao et al. (2011) found that the outer wind structures that evolved in their simulations depended much less on the initial condition than on the model physics being employed.

This sensitivity to the MP, however, emerged owing to how hydrometeors in different schemes interacted with radiative processes, i.e., cloud-radiative forcing (CRF). Fovell et al. (2010a) demonstrated that the motion and structural variation in their MP ensemble disappeared when clouds were made transparent to radiation in their semi-idealized simulations employing the Weather Research and Forecasting (WRF) model's Advanced Research WRF (ARW) core. MP schemes differ with respect to the amounts and relative distributions of hydrometeors, such as cloud ice, snow,

cloud droplets, etc. (Fovell et al. 2010b). These particles have different effective sizes (e.g., Dudhia 1989) that determine how they interact with longwave (LW) and shortwave (SW) radiation.

The CRF signal consists of prominent LW cooling along the anvil cloud top, weaker LW warming within the cloud, and absorption of SW radiation in the upper layer of the anvil when the sun is above the horizon. This is illustrated in Fig. 1a, taken from Bu et al. (2014), which used a semi-idealized version of the operational Hurricane WRF (HWRF) model to demonstrate how and why CRF influences storm structure. Note the condensate field (shaded) is thinner and radially less extensive when CRF is inactive (1b). The CRF-off simulation still has clear-sky radiative processes, but treats clouds as transparent. The CRF-on run's wind field is considerably broader (2), which has important implications for the storm surge threat, and track.

Bu et al. (2014) found that the cloud-top cooling component of CRF contributed little to widening the storm and removing it produced results nearly indistinguishable from the CRF-off case (not shown). Instead, the in-cloud LW warming was demonstrated as being the important ingredient. Bu et al. (2014) explained that this relatively small but persistent diabatic forcing encouraged gentle ascent that eventually led to enhanced convective activity in the outer region. This resulted in considerably enhanced heating associated with condensation, which directly led to radial expansion of the wind field. Through even more idealized experimentation, Bu et al. (2014) and Fovell and co authors (2015) conclusively proved that the weak LW warming played an active role in determining storm expansion and width by imposing the diurnally-averaged CRF as an external forcing and manipulating its radial extent. Storm width quickly became as large as, but no wider than, the imposed LW warming field.

The simulations described above used the RRTMG radiation scheme, which is commonly employed in WRF-ARW but was only recently implemented in the HWRF system. Another finding of Bu et al. (2014) was that the radiation scheme employed operationally in the HWRF model, which originated at GFDL, had little recognizable CRF, and functioned as a CRF-off run. (See Fig. 2, wind profile marked "GFDL".) This suggests that, other factors being equal, that HWRF might possess a negative size bias; lacking a mechanism for further promoting the development of outer convection, their storms should be too radially compact.

2. The DTC microphysics and radiation ensemble

The DTC conducted physics testing of the HWRF model utilizing 2012 Atlantic and East Pacific TCs, using the 2013 operational version (L. Bernardet and M. Biswas, personal communication). Included were ensemble members using the Thompson microphysics and RRTMG radiation schemes (designated HDTR or HD2R, depending on the radiation time step), which were candidates for adoption by the operational model. This physics combination, however, was found to have generally degraded skill relative to the operational HWRF configuration of Ferrier MP and GFDL radiation (designated HD35) and, as a consequence, was not adopted. Furthermore, there were distinct contrasts between the Atlantic (ATL) and East Pacific (EPAC) results.

For example, HDTR showed slightly improved track error relative to the control in the ATL (not shown), but at the cost of significantly degraded position skill in EPAC (Fig. 3). The mean error (ME) difference between HDTR and HC35 in that basin was particularly large after about 60 h. In this basin, HDTR storms tended to track to the right of the control cases (not shown) and also move too quickly, as illustrated by the along-track error shown in Fig. 4. This contrasts with the ATL basin, in which the HDTR cases had a smaller negative along track speed bias relative to the operational configuration's storms (Fig. 5), and tracked to their left (not shown).

The DTC analysis also uncovered size biases that were opposite in sign between the two basins. In the ATL (Fig. 6), the HDTR physics made the storms wider than in the control runs, while in the EPAC its storms were smaller (although both were larger than observed for most forecast hours). In the EPAC, intensity error started out small for both HDTR and HD35, but quickly became significantly negative for the former after forecast hour 30 (not shown). In contrast, the bias of HDTR in the ATL basin was positive after hour 6, being worse than the control prior to hour 54 and better after that (not shown). Thus, it was apparent there is likely no simple answer to why and how the HDTR storms behave and evolve relative to those in the control configuration.

3. Work performed

a. Initial exploration

The PI and graduate student Yizhe Peggy Bu visited DTC for several weeks during summer of 2014. During that period, we were given access to some of the ensemble model output, and perused the information available at `http://www.dtcenter.org/eval/hwrf_hc35_hdtr/verify/`. We started by concentrating on comparing HDTR and HC35 storm sizes, via visual inspection, irrespective of which was more congruent with the observations. In the ATL basin, based on a rough average of the four storm quadrants, 10 of 12 cases examined suggested HDTR storms were larger, with the other two storms being judged as being the same. Among the 12 EPAC cases examined, 7 HDTR storms were deemed smaller than their HC35 counterparts, with only three being clearly larger.

Storm size can directly and indirectly impact TC motion. Two principal contributions to TC motion are external steering and beta drift. The latter exists owing to the latitudinal gradient of planetary vorticity, and is strongly sensitive to the strength of the winds in the storm's outer region [beyond roughly 250 km; Fiorino and Elsberry (1989)]. Other factors being equal, a storm that is relatively wider will have a larger northwestward component in its motion. Therefore, for a westbound TC, one with a radially broader wind field would be expected to develop a more northward motion, tracking to the right of a narrower storm. In the EPAC, where SST often decreases rapidly to the north, small position errors can result in substantial intensity biases. It might be surmised a model storm that is too wide might venture too close to these cold waters.

EPAC hurricane Daniel was selected as a representative member of the EPAC cases. HDTR's track error (Fig. 8) grew rapidly relative to the control run's after 42 h. The Thompson/RRTMG storm (labeled HD2R on the figure) tracked to the right of both the best track and HC35 (Fig. 9), winding up over colder SSTs, resulting in a large negative intensity bias. However, like most EPAC cases, the Thompson/RRTMG combination apparently resulted in a *smaller* storm. This appears to contradict our expectations.

From the HWRF model output from the first Daniel run, initialized 2012070406, we constructed vortex-following storm composites, which can be further subdivided into symmetric and asymmetric

parts. Figure 10 shows the radial profiles of the symmetric component of the horizontal wind field at 2 km above mean sea level (MSL) for the control run (HC35, labeled F/GFDL), a simulation using Ferrier MP with RRTMG radiation (labeled F/RRTMG and HD3R), and the Thompson/RRTMG case HD2R, averaged between forecast hours 30 and 36. At this level and at this time, the HD2R storm is less well developed but had stronger winds beyond 120 km from the center. Therefore, by this metric, the Thompson/RRTMG TC was actually not narrower.

The beta drift is influenced by the tangential winds through the storm's depth, so assessing it based on the 10-m MSL wind alone could prove deceiving, as this particular case illustrates. Figure 11 shows the symmetric components of the tangential (contoured) and radial wind (colored) for the three simulations, averaged between hours 36 and 42. The Thompson/RRTMG storm remained less organized but wider. The track divergence appeared after this time, and we believe that HD2R's slightly stronger outer winds helped contribute to this. Subsequently, the Thompson/RRTMG storms became demonstrably narrower at all levels (not shown), but this was *after* the cold SSTs negatively impacted storm intensity.

b. Hypothesis and analysis

Our previous research, summarized above, showed that replacing GFDL radiation with RRTMG should encourage wider model storms to develop, other factors being equal. Our examination of the HWRF model output suggested that another model parameter influencing storm width was "gfs_alpha". This parameter was added to HWRF's GFS planetary boundary layer (PBL) scheme by Gopalakrishnan et al. (2013), motivated by PBL and eddy mixing observations of Zhang et al. (2011). This technique involved adding a factor $0 \leq \alpha \leq 1$ to the line of code that determines the vertical structure and magnitude of eddy mixing K_m, and was designed to prevent the development of unrealistically deep PBL depths in the hurricane inner core (reflecting overly large mixing).

Using an older version of HWRF, Gopalakrishnan et al. (2013) determined that $\alpha = 0.25$ generated PBL depths that were most comparable to those seen in the Zhang et al. (2011) study. The value of α adopted in the 2013 HWRF model, however, was $\alpha = 0.7$. This value was found to be associated with the largest model skill.

Using semi-idealized HWRF simulations, we investigated the influence of gfs_alpha on storm width, in combination with CRF. While we included Thompson MP in our tests, we concentrated on experiments using the operational Ferrier scheme, to reduce the number of degrees of freedom. Figure 12 shows symmetric components of 10-m wind speed from four simulations using the Ferrier with either GFDL or RRTMG radiation, and with $\alpha = 0.25$ or 0.7. The averaging period was between hours 72 and 96.

As shown by Bu et al. (2014), the F/GFDL simulations are effectively CRF-off runs. It is seen that both CRF and larger α radially expand the storm, with the widest widths resulting when large α was employed with CRF active. Indeed, the 34-kt wind radius (R34) varies by a factor of 2 among the runs, a substantial variation given all simulations commenced with identical initial conditions. The narrowest TC is the F/GFDL/α=0, with an R34 of about 120 km, while the widest was F/RRTMG/α=0.7, with an R34 of 225 km.

Indeed, our assessment is that the dependence of storm width on vertical mixing is even larger than that on in-cloud LW warming. Figure 13 compares diabatic heating (DH) owing to microphysics for simulations differing by CRF. The DH difference field (colored field, at bottom) reveals that the CRF-on storm (top panel) generated more heating over a radially more extensive region, resulting in a radially more extensive tangential wind field (contoured field, at bottom). The difference in microphysics DH is even more stark when α is changed from 0.7 to 0.25 (Fig. 14). The larger α storm's tangential wind field is stronger over a wider area and deeper depth.

Our interpretation of these results is as follows: By itself, cloud-radiative forcing results in wider storms, potentially influencing track and even intensity. The HWRF model's GFDL scheme had little to no effective CRF, as demonstrated by Bu et al. (2014). The optimal value of the gfs_alpha parameter, α, is around 0.25, according to Gopalakrishnan et al. (2013). That study showed that values larger than 0.25 make the inner core PBL depth too large, with a substantial impact on intensity. However, the value of α selected for operational use was larger, 0.7. We find this value not only impacts intensity, but also storm width. The larger α value may have been chosen because the model's radiation scheme was not effective, and the HWRF model had been producing storms that were too narrow.

Thus, when the RRTMG scheme was adopted, we believe the combination of CRF and large

α resulted in storms that were too wide. That result was clear in the ATL basin, but initially appeared to be contradicted in the EPAC. However, the dominance of negative size biases in the EPAC for RRTMG cases appeared to be an illusion. Many of those storms actually had positive size biases early on that, owing to larger beta drift, resulted in tracks that moved the TCs towards unfavorable SSTs. It was only after the storms were weakened by passage over colder waters that the storms weakened in intensity and shrunk in size.

In other words, our suggestion is that the relatively large α parameter value used operationally was inadvertently compensating for the lack of effective CRF in the HWRF model when GFDL radiation was used. As a consequence, our recommendation was to reduce α to a value more consistent with the observations when the RRTMG package is adopted.

c. How and why α controls storm width

The next step was to understand how and why the α parameter influences radial storm extent. As designed by Gopalakrishnan et al. (2013), decreasing α reduces the magnitude of eddy mixing, as applied to both momentum (K_m) as well as to temperature and moisture (K_h) fields. That is seen in our experiments (Fig. 15); note how much larger the K_m values are in the $\alpha = 0.7$ cases (top row). One thing larger vertical mixing does is alter the vertical transport of water vapor. From the equations, we can anticipate increasing K_m results in relatively larger vapor content above, and lower content below, the level of maximum eddy mixing. That is what was found in this experiment, as illustrated in Fig. 16, which shows vertical profiles of water vapor mixing ratio averaged over radii to 240 km outward from the core.

From these results, we hypothesize that CRF and PBL eddy mixing influence storm width for different but complementary reasons. As discussed in Bu et al. (2014), LW warming within the extended anvil induces gentle but persistent upward motion, ultimately resulting in enhanced convective activity in the TC outer core. The diabatic forcing associated with the convection, which substantially exceeds that of the LW forcing, causes the wind field to broaden, in the manner investigated in studies such as Holland and Merrill (1984) and Hack and Schubert (1986). We see that enhanced vertical eddy mixing represents another avenue for enhancing outer core convective heat-

ing, by lofting vapor to the top of the boundary layer. In this way, it emerges that excessively large mixing (compared to the available observations) could have been compensating for inappropriately transparent clouds in previous versions of the operational HWRF model.

d. Contributions to the operational model resulting from this work

This work directly led to HWRF code alterations that have been incorporated into the 2015 version. First of all, identifying the likely source of the issues revealed in the DTC experiment resulted in the RRTMG scheme being a more viable candidate for incorporation into the operational HWRF physics package (as occurred in the 2015 HWRF, for example). Once we recognized that α was an important size-controlling parameter, we realized that the way the eddy mixing reduction was being incorporated into the GFS PBL scheme could be refined. As noted above, previous studies suggested that smaller values of α were appropriate, but this result was specific to the hurricane inner core, where wind speeds are large. As implemented prior to 2015, the selected α value, whatever it was, was being applied throughout the model – including outside the hurricane core, at lower wind speeds, and even over land. It seemed prudent to devise a revised scheme that targets the reduced α values only where they are at least somewhat supported by the available observations.

Our "variable α" algorithm attempts to restrict the artificial reduction of eddy mixing only to higher wind situations as would be found in the hurricane inner core. Using the Zhang et al. (2011) data, we define a maximum value of K_m approrpriate given the wind speed simulated at 500 m MSL. [This is because the Zhang et al. (2011) calculations were mainly made at that level.] If the value of K_m produced by the GFS PBL scheme with $\alpha = 1$ does not exceed this upper bound, or the grid column resides over land, no further modification is made. If the value of K_m generated by the PBL scheme does exceed the upper bound – and this is likely to occur only with the fast winds of the inner core – the value is limited in conformance with the observations.

This modification to the GFS PBL was tested by EMC and selected for inclusion in the 2015 HWRF.

REFERENCES

Braun, S. A. and W.-K. Tao, 2000: Sensitivity of high-resolution simulations of Hurricane Bob (1991) to planetary boundary layer parameterizations. *Mon. Wea. Rev.*, **128**, 3941–3961.

Bu, Y. P., R. G. Fovell, and K. L. Corbosiero, 2014: Influence of cloud-radiative forcing on tropical cyclone structure. *J. Atmos. Sci.*, **71**, 1644–1662, doi:10.1175/JAS-D-13-0265.1.

Cao, Y., R. G. Fovell, and K. L. Corbosiero, 2011: Tropical cyclone track and structure sensitivity to initialization in idealized simulations: A preliminary study. *Terrestrial, Atmopsheric and Oceanic Sciences*, **22**, 559–578, doi:10.3319/TAO.2011.05.12.01(TM)1.

Dudhia, J., 1989: Numerical study of convection observed during the winter monsoon experiment using a mesoscale two-dimensional model. *J. Atmos. Sci.*, **46**, 3077–3107.

Fiorino, M. J. and R. L. Elsberry, 1989: Some aspects of vortex structure related to tropical cyclone motion. *J. Atmos. Sci.*, **46**, 975–990.

Fovell, R. G. and co authors, 2015: Influence of cloud microphysics and radiation on tropical cyclone structure and motion. *Multiscale Convection-Coupled Systems in the Tropics*, Amer. Meteor. Soc., Meteor. Monogr., in press.

Fovell, R. G., K. Corbosiero, and H.-C. Kuo, 2010b: Influence of cloud-radiative feedback on tropical cyclone motion: Symmetric contributions. *29th Conf. on Hurricanes and Tropical Meteorology*, American Meteorological Society.

Fovell, R. G., K. L. Corbosiero, and H.-C. Kuo, 2009: Cloud microphysics impact on hurricane track as revealed in idealized experiments. *J. Atmos. Sci.*, **66**, 1764–1778, doi:10.1175/2008JAS2874.1.

Fovell, R. G., K. L. Corbosiero., A. Seifert, and K. N. Liou, 2010a: Impact of cloud-radiative processes on hurricane track. *Geophys. Res. Lett.*, **37 (7)**, doi:10.1029/2010GL042691.

Fovell, R. G. and H. Su, 2007: Impact of cloud microphysics on hurricane track forecasts. *Geophys. Res. Lett.*, **134**, L24810, doi:10.1029/2007GL031723.

Gopalakrishnan, S. G., F. D. Marks, J. A. Zhang, X. Zhang, J.-W. Bao, and V. Tallapragada, 2013: A study of the impacts of vertical diffusion on the structure and intensity of the tropical cyclones using the high-resolution HWRF system. *J. Atmos. Sci.*, **70**, 524–541.

Hack, J. J. and W. H. Schubert, 1986: Nonlinear response of atmospheric vortices to heating by organized cumulus convection. *J. Atmos. Sci.*, **43**, 1559–1573, doi:10.1175/1520-0469(1986)043⟨1559:NROAVT⟩2.0.CO;2.

Holland, G. J., 1983: Tropical cyclone motion: Environmental interaction plus a beta effect. *J. Atmos. Sci.*, **40**, 328–342.

Holland, G. J. and R. T. Merrill, 1984: On the dynamics of tropical cyclone structural changes. *Quart. J. Roy. Meteor. Soc.*, **110**, 723–745.

Lord, S. J., H. E. Willoughby, and J. M. Piotrowicz, 1984: Role of a parameterized ice-phase microphysics in an axisymmetric, nonhydrostatic tropical cyclone model. *J. Atmos. Sci.*, **41**, 2836–2848.

Wang, Y., 2002: An explicit simulation of tropical cyclones with a triply nested movable mesh primitive equation model: TCM3. Part II: Model refinements and sensitivity to cloud microphysics parameterization. *Mon. Wea. Rev.*, **130**, 3022–3036.

Zhang, J. A., R. F. Rogers, D. S. Nolan, and F. D. Marks, 2011: On the characteristic height scales of the hurricane boundary layer. *Mon. Wea. Rev.*, **139**, 2523–2535.

Zhu, T. and D.-L. Zhang, 2006: Numerical simulation of hurricane Bonnie (1998). Part II: Sensitivity to varying cloud microphysical processes. *J. Atmos. Sci.*, **63**, 109–126.

List of Figures

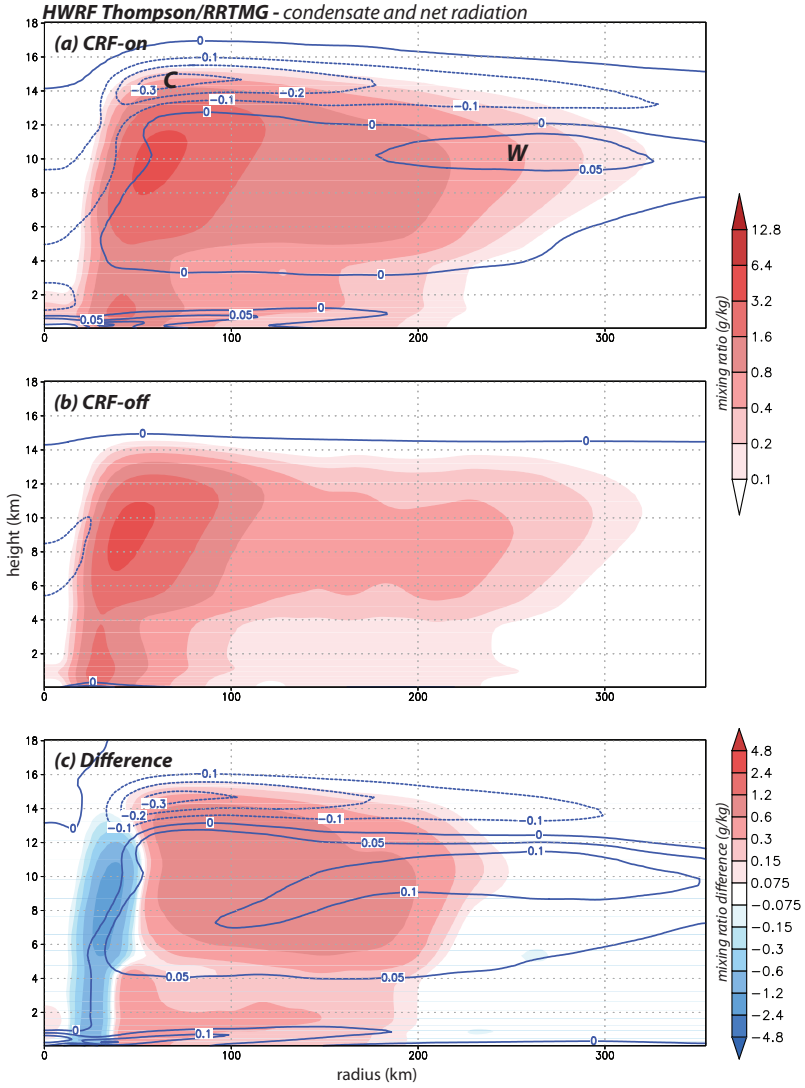

FIG. 1. Radius vs. height cross-sections showing the symmetric components of total condensate (shaded, note logarithmic scale) and net radiative forcing (negative [dashed] contour interval 0.1 K h^{-1}, and positive [solid] interval 0.05 K h^{-1}) field. "Radiative forcing" refers to the potential temperature tendency owing to radiative processes. Letters "C" and "W" highlight local maxima of diabatic cooling and warming, respectively. From Bu et al. (2014).

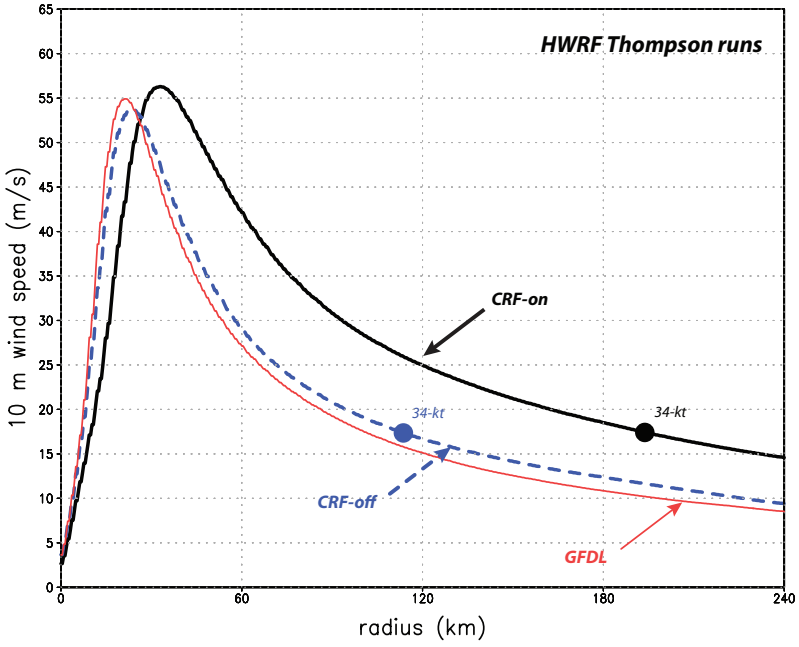

FIG. 2. Radial profiles of the azimuthally-averaged 10 m wind speed from the HWRF day 4 composite, computed from D3. The Thompson/RRTMG CRF-on and CRF-off simulations are shown, along with a Thompson simulation made using the HWRF GFDL radiation scheme. Radii of the 34-kt (17.5 m s^{-1}) wind indicated. From Bu et al. (2014).

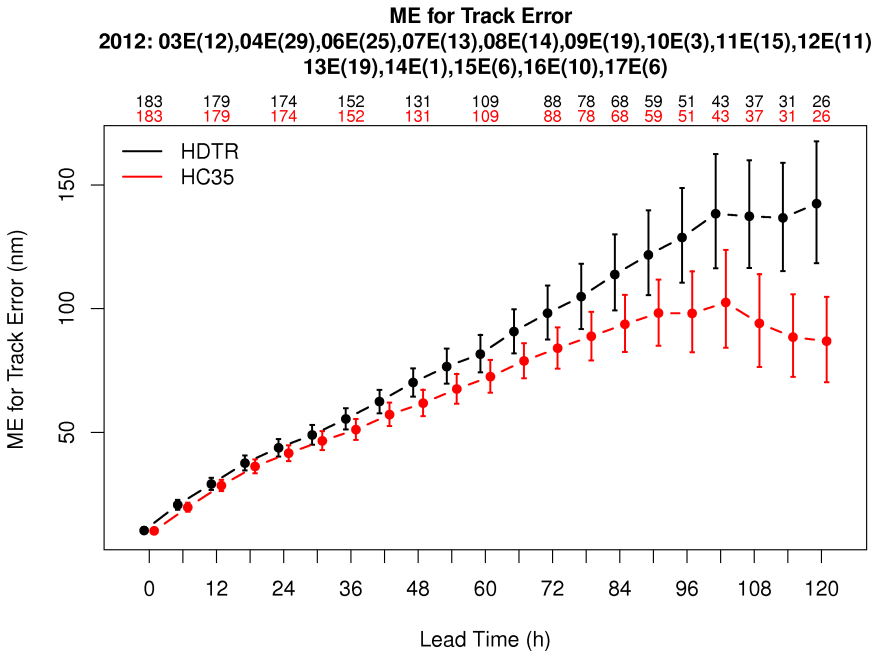

FIG. 3. Mean error (ME) for track error for EPAC cases from the DTC HC35-HDTR experiment. From a presentation by Bernardet et al..

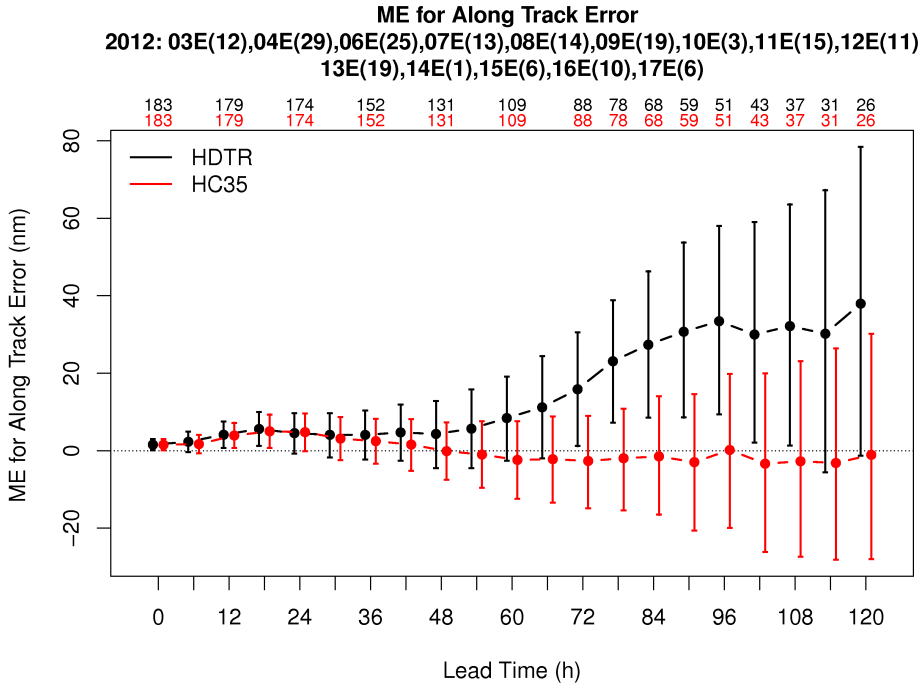

FIG. 4. As in Fig. 3, but for EPAC along track error. From a presentation by Bernardet et al..

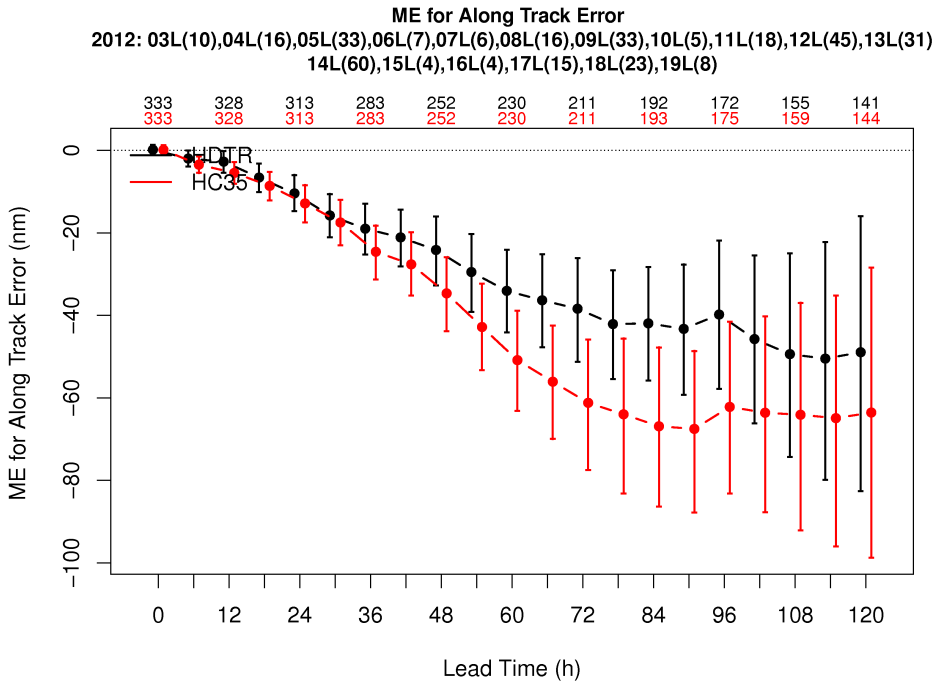

FIG. 5. As in Fig. 3, but for ATL along track error. From a presentation by Bernardet et al..

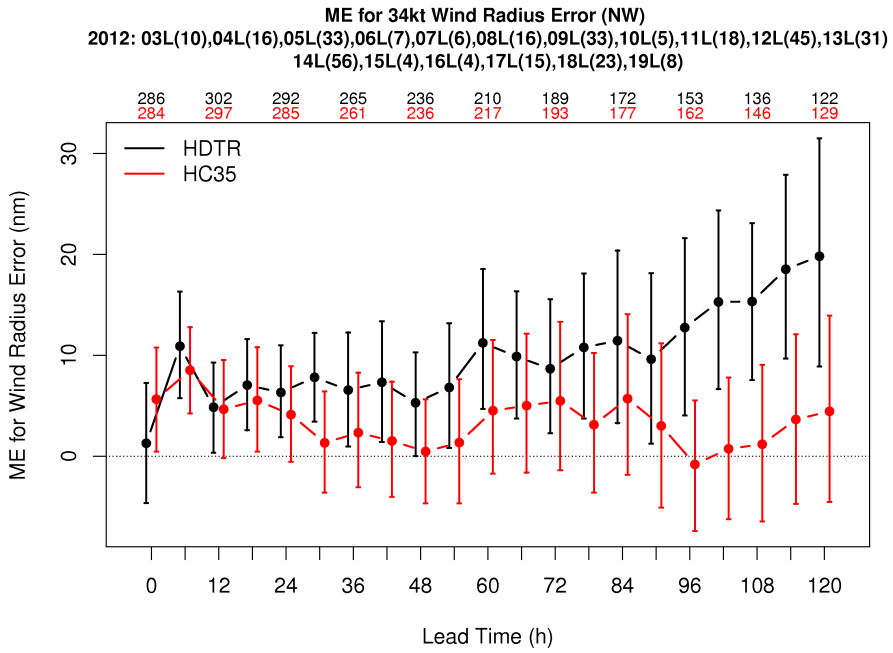

FIG. 6. As in Fig. 3, but for ATL 34-kt wind radius error. From a presentation by Bernardet et al..

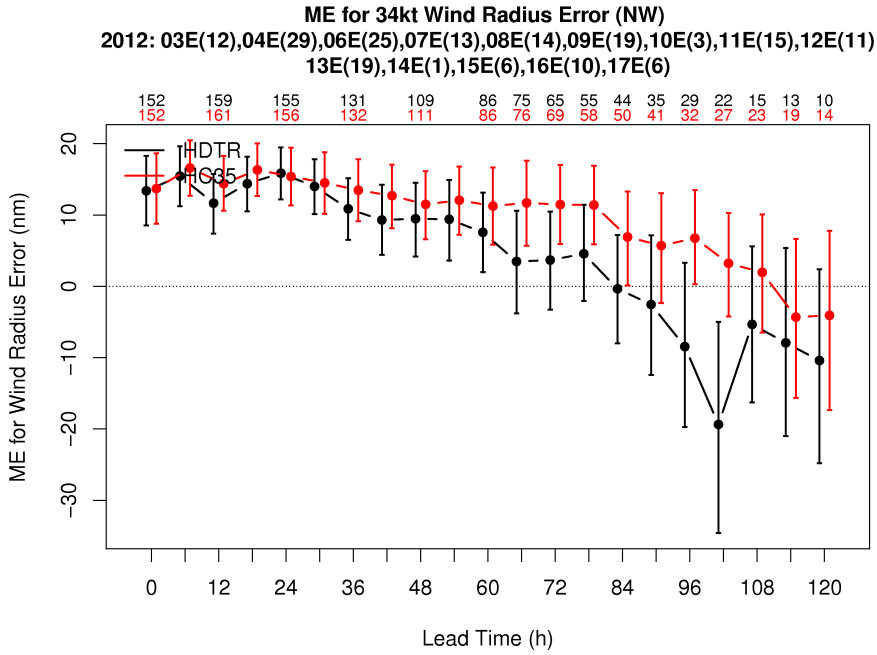

FIG. 7. As in Fig. 3, but for EPAC 34-kt wind radius error. From a presentation by Bernardet et al..

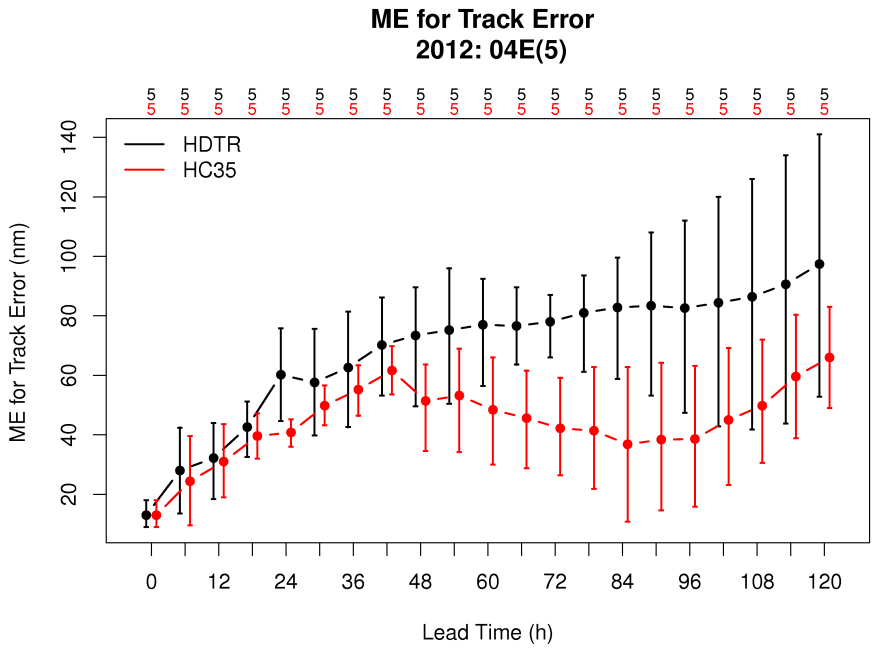

FIG. 8. As in Fig. 3, but for EPAC case Daniel. From a presentation by Bernardet et al..

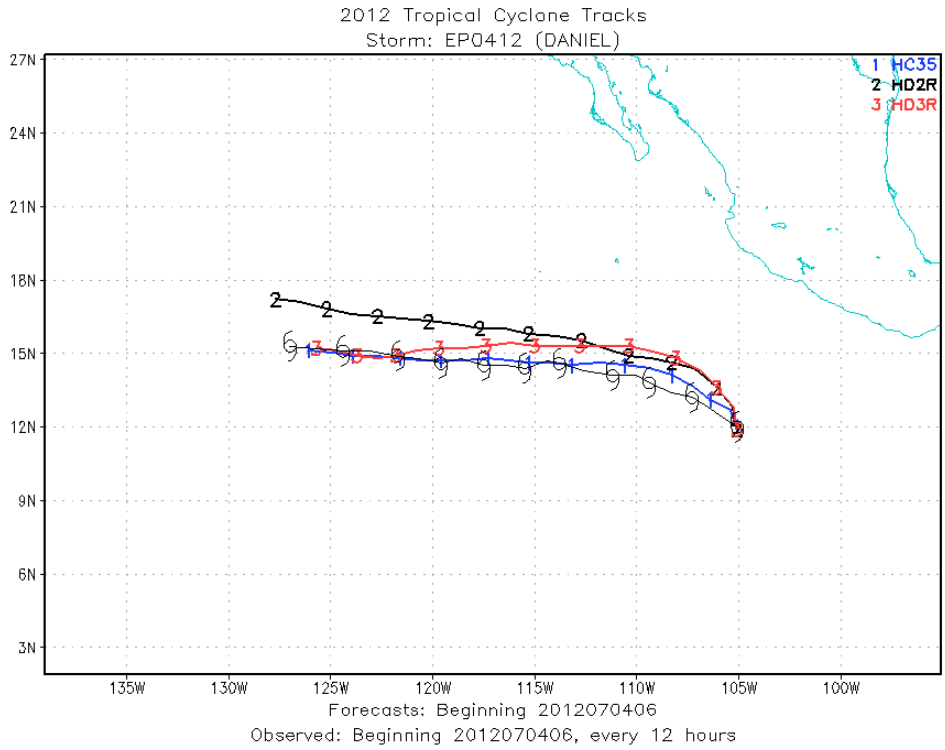

FIG. 9. Tracks for EPAC case Daniel, with positions marked every 12 hours. HD2R is HDTR with a different radiation time step. HD3R used Ferrier MP with RRTMG radiation. Hurricane symbols denote best track. From DTC.

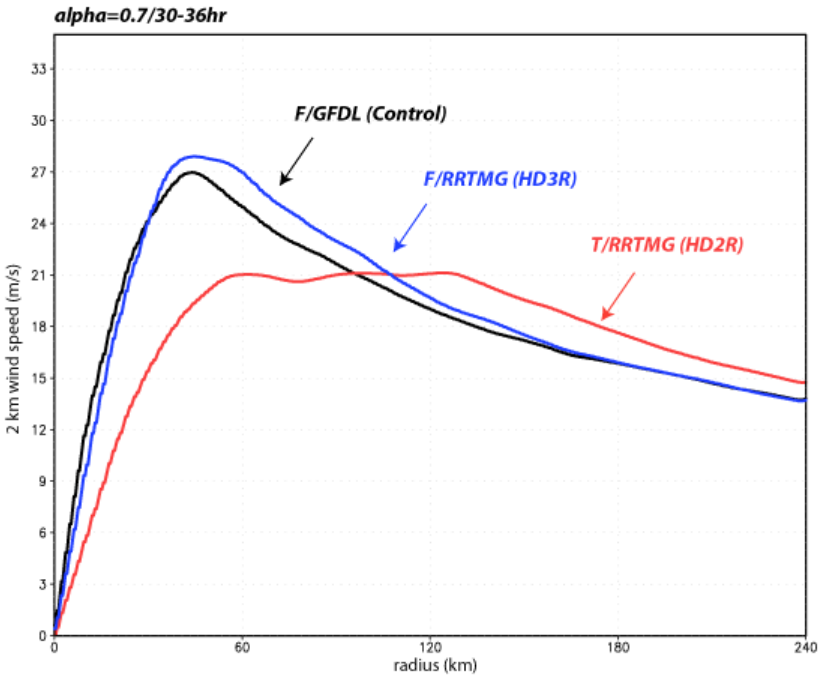

FIG. 10. Symmetric components of horizontal wind at 2 km MSL, averaged between forecast hours 30 and 36, from Hurricane Daniel simulations Control (HC35), HD2R and HC3R.

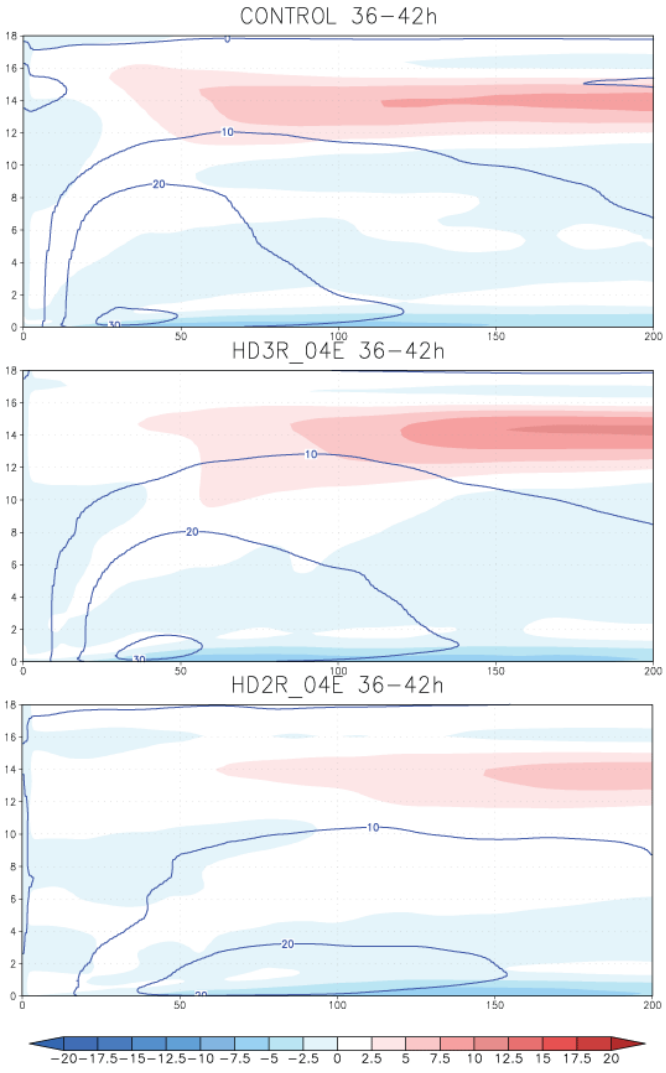

FIG. 11. Radius vs. height composites of the symmetric component of tangential (contoured) and radial (colored) wind, averaged between forecast hours 36 and 42, from Hurricane Daniel simulations Control (HC35), HD2R and HC3R.

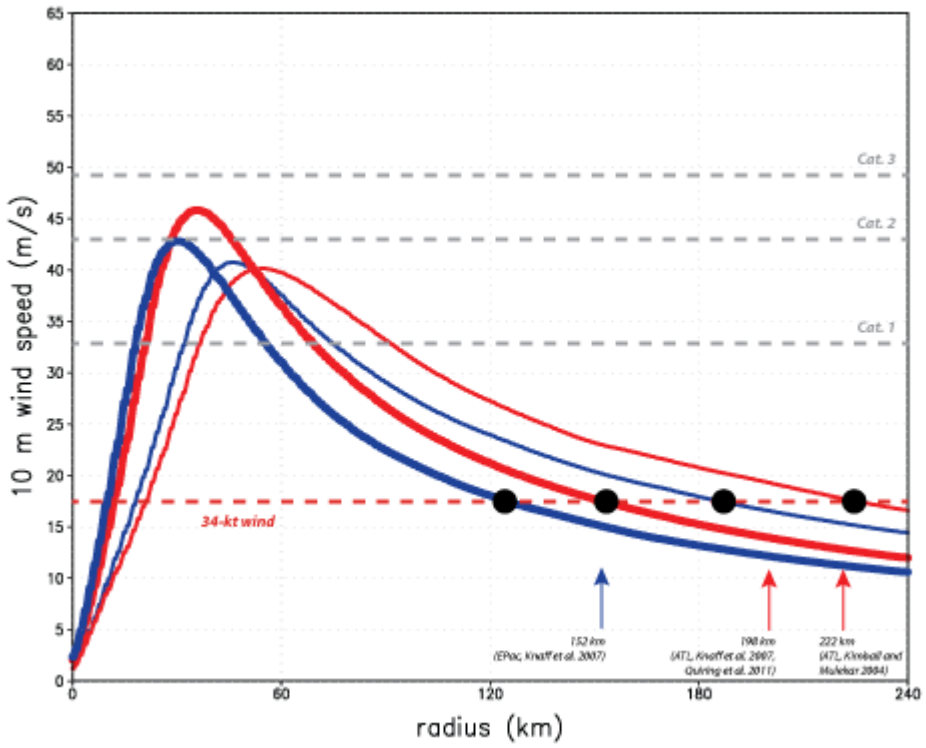

FIG. 12. Symmetric components of horizontal wind from averaged between forecast hours 72 and 96 for semi-idealized simulations using Ferrier MP and either GFDL or RRTMG radiation with $\alpha = 0.25$ or 0.7. Thick blue: F/GFDL/α=0.25; thin blue: F/GFDL/α=0.7; thick red: F/RRTMG/α=0.25; thin red: F/RRTMG/α=0.7. RRTMG may be referred to as RRTM in figure labels.

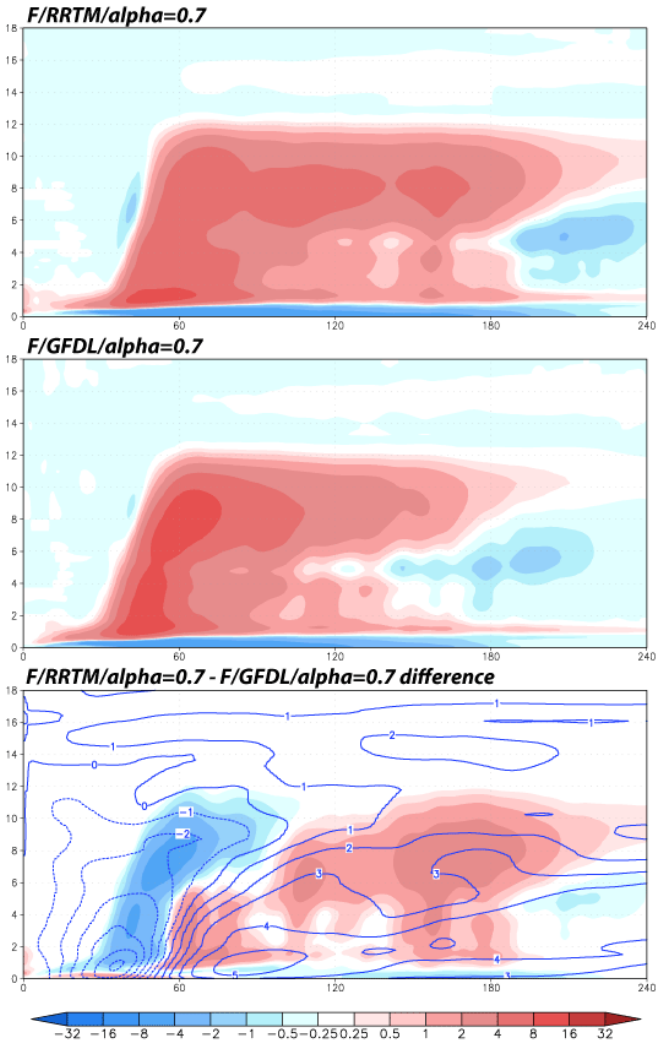

FIG. 13. Radius-height profiles of the symmetric components of diabatic heating from microphysics (colored) from semi-idealized simulations for (a) F/RRTMG/α=0.7, (b) F/GFDL/α=0.7, and (c) the difference field between the two. Bottom panel also includes tangential wind field difference field (contoured). This comparison is between simulations that vary owing to CRF.

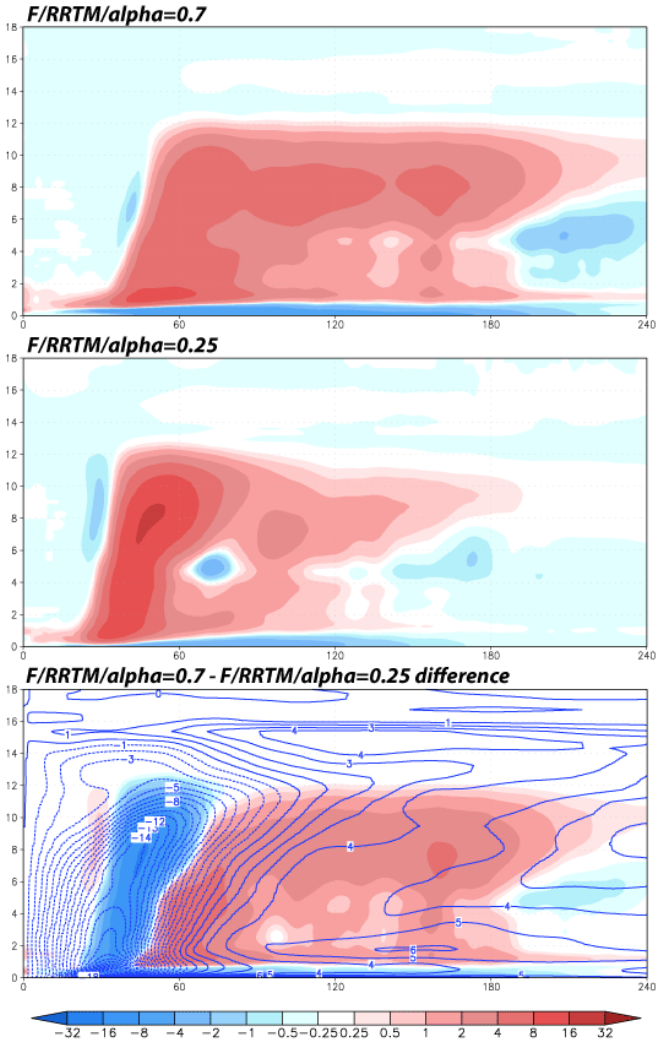

FIG. 14. As in Fig. 13, but for simulations F/RRTMG/α=0.7 and F/RRTMG/α=0.25. This comparison is between simulations that vary owing to the α parameter.

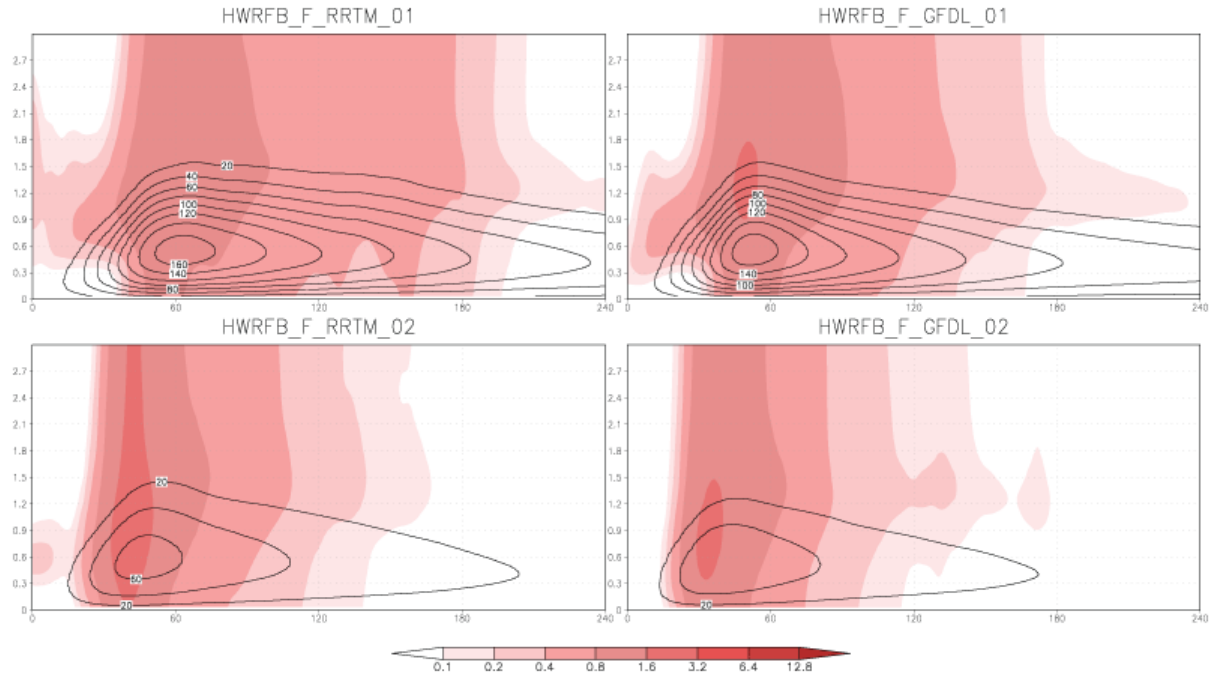

FIG. 15. Radius-height sections of total condensate (colored) and eddy mixing coefficient K_m (contoured) for semi-idealized Ferrier simulations using RRTMG (left column) and GFDL (right column), with $\alpha = 0.7$ (top row) and 0.25 (bottom row). Symmetric components averaged between hours 72 and 96.

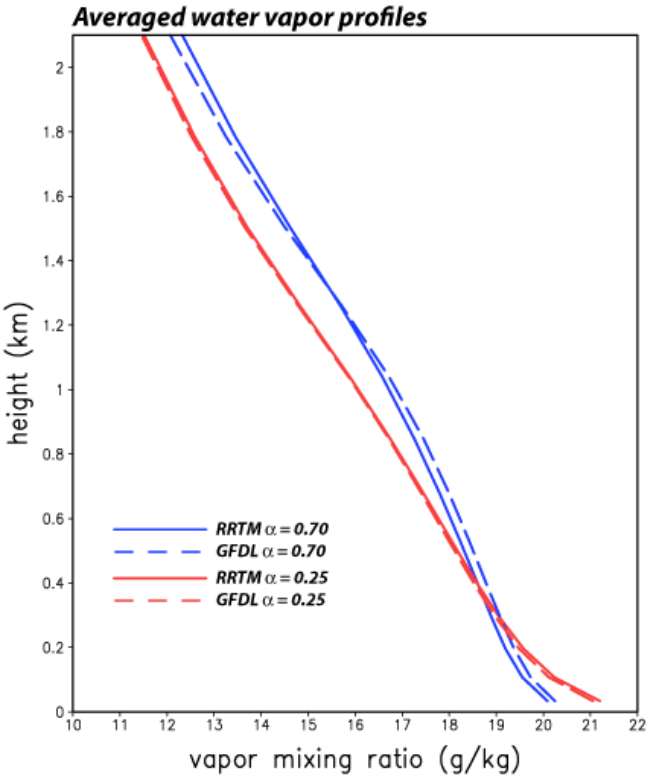

FIG. 16. Vertical profiles of radially, temporally and azimuthally averaged water vapor profiles, from RRTMG and GFDL simulations using larger and smaller α values. Averaged between hours 72 and 96.